Electronic Supplementary Material (ESI) for Catalysis Science & Technology.

The Role of Catalyst-Support Interactions in Oxygen Evolution Anodes based on $Co(OH)_2$ Nanoparticles and Carbon Microfibers

Laura Mallón,[a,b] Nuria Romero,[a] Alicia Jiménez,[c] Elena Martín-Morales,[a,b] José Alemán,[d] Rubén Mas-Ballesté,[c] Roger Bofill,[a] Karine Philippot,*[b] Jordi García-Antón,*[a] Xavier Sala*[a]

[a] *Departament de Química, Universitat Autònoma de Barcelona, Cerdanyola del Vallès, 08193 Barcelona, Spain. Email. xavier.sala@uab.cat*

[b] CNRS, LCC (Laboratoire de Chimie de Coordination), UPR8241, Université de Toulouse, UPS, INPT, F-31077 Toulouse cedex 4, France

[a] *Department of Inorganic Chemistry (module 07), Facultad de Ciencias, Universidad Autónoma de Madrid, Madrid, Spain*

[b] Department of Organic Chemistry (módulo 01), Facultad de Ciencias, Universidad Autónoma de Madrid, Madrid, Spain

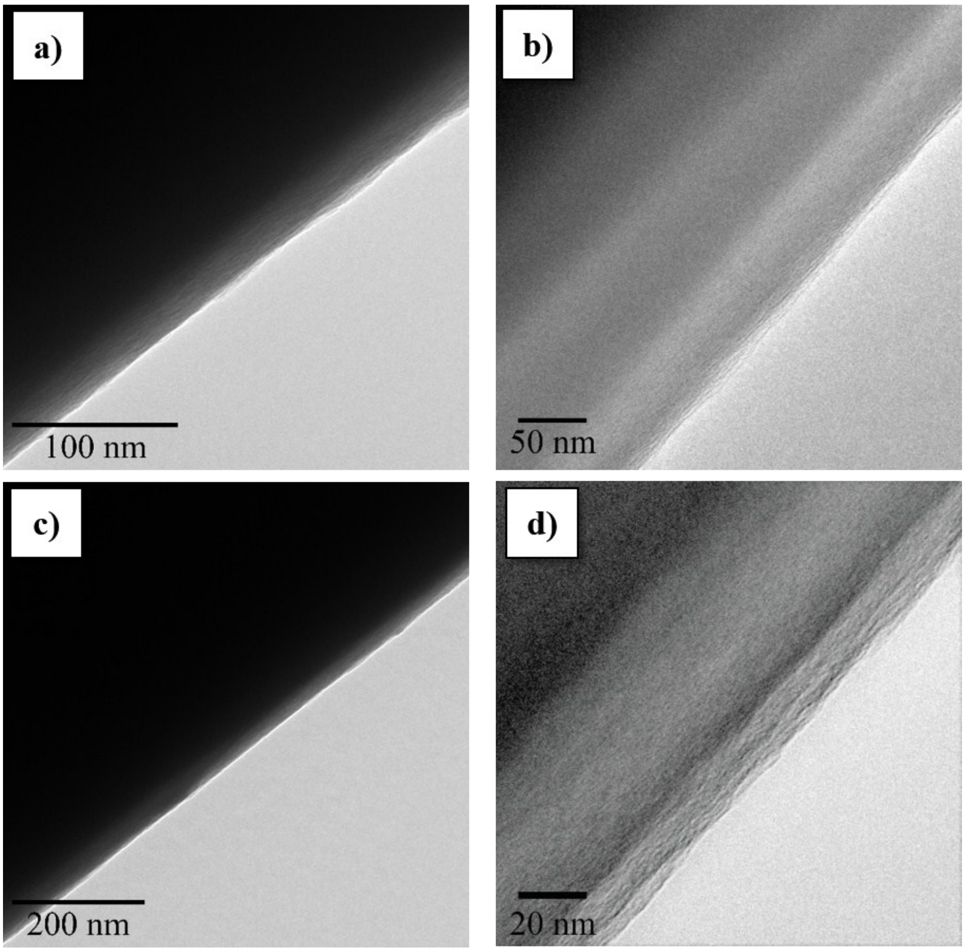

Figure S1. TEM images of the as-synthesized CF (a and b) and ox-CF (c and d) before the deposition of Co-based nanoparticles onto their surface.

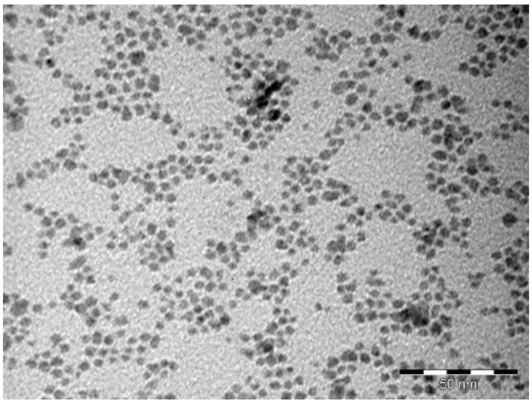

Figure S2. TEM images of colloidal Co NPs in 1-heptanol **(Co^{heptOH}NPs)** prepared following our reported methodology.[1]

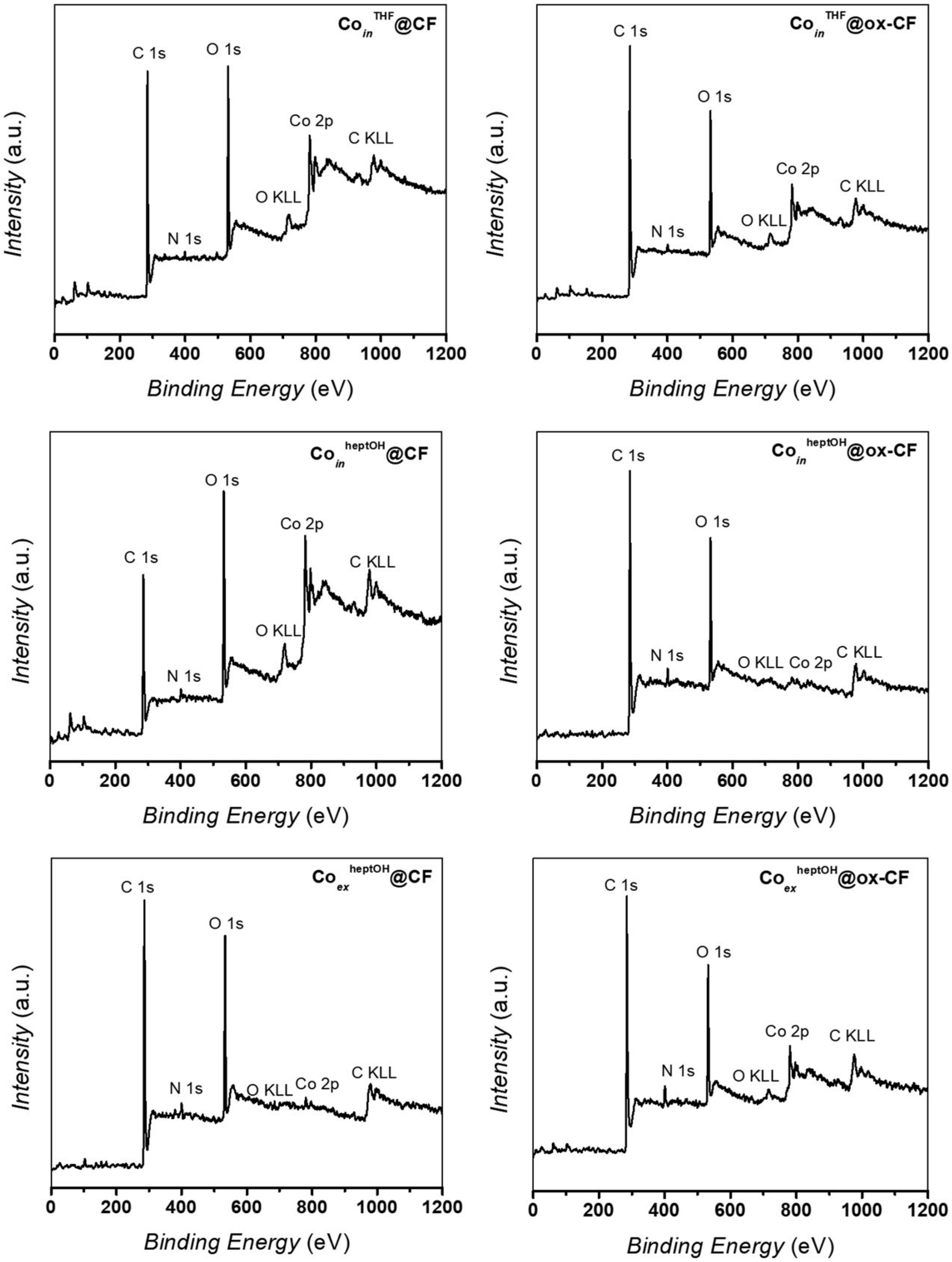

Figure S3. XPS data of all the synthesized hybrid materials. The main peaks are indeed to O 1s, N 1s and C 1s regions (O KLL represents the energy of the electrons ejected from the atoms due to the filling of the O1s state (K shell) by an electron from the L shell coupled with the ejection of an electron from an L shell).

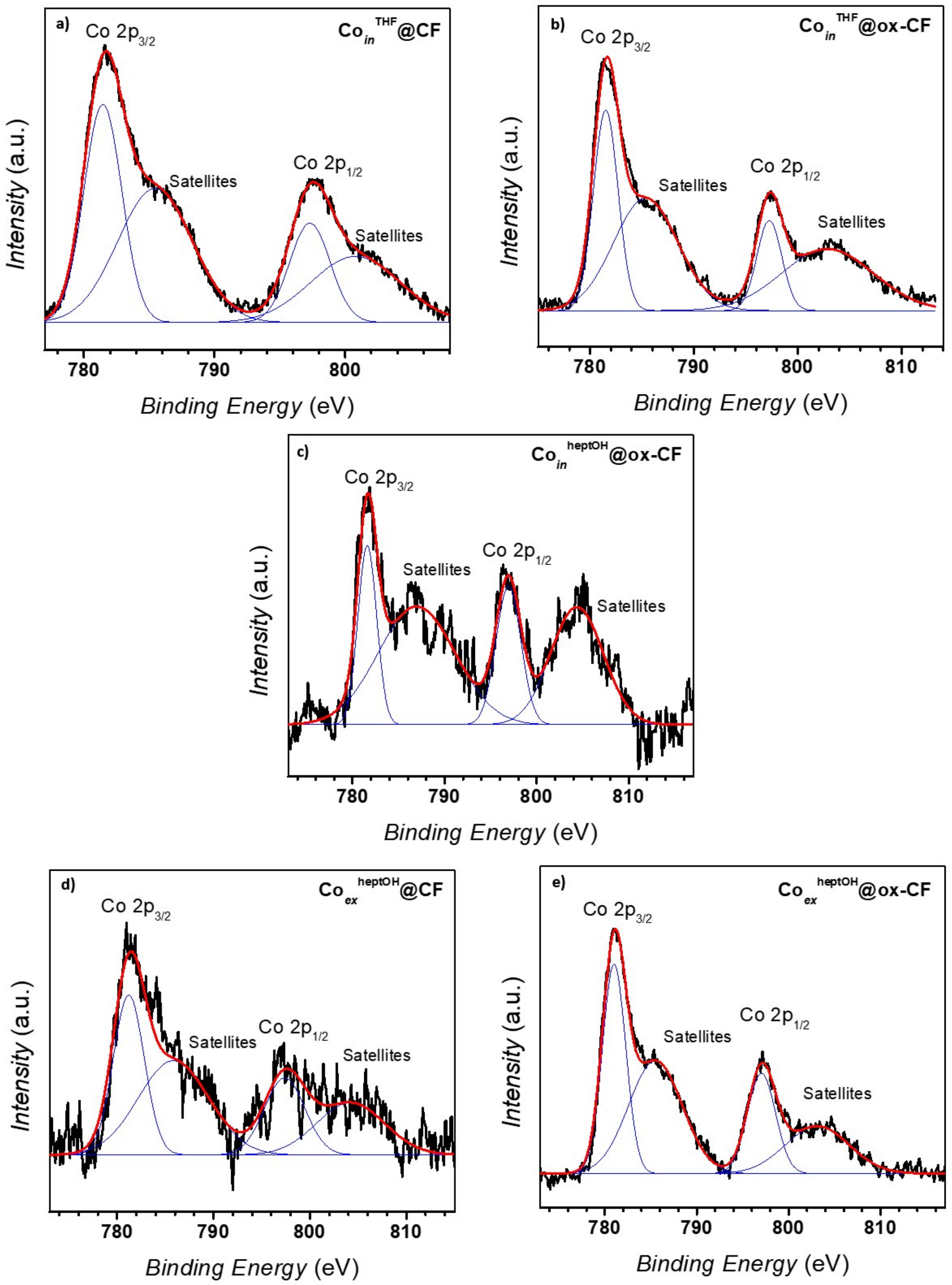

Figure S4. High-resolution XPS analysis in the Co 2p region of a) **Co$_{in}^{THF}$@CF**, b) **Co$_{in}^{THF}$@ox-CF**, c) **Co$_{in}^{heptOH}$@ox-CF**, d) **Co$_{ex}^{heptOH}$@CF** and e) **Co$_{ex}^{heptOH}$@ox-CF**.

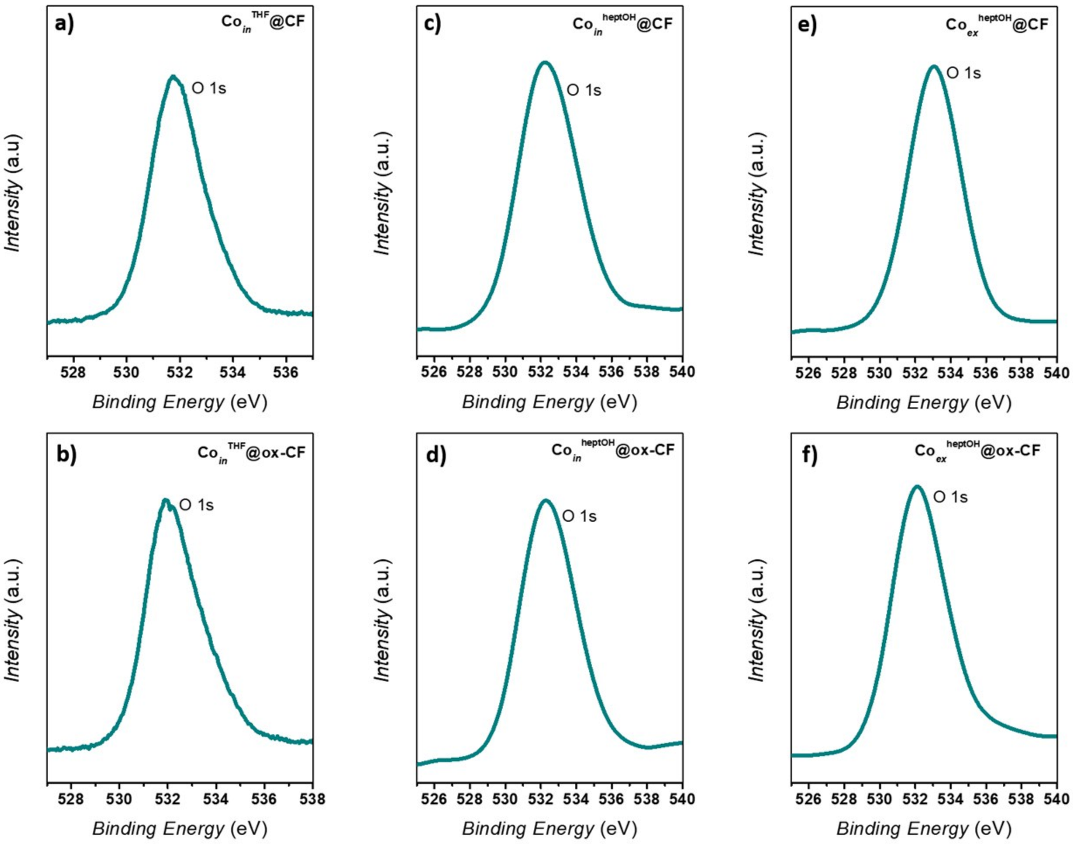

Figure S5. XPS high-resolution spectra in the O 1s region of the a) **Co$_{in}^{\text{THF}}$@CF**, b) **Co$_{in}^{\text{THF}}$@ox-CF**, c) **Co$_{in}^{\text{heptOH}}$@CF,** d) **Co$_{in}^{\text{heptOH}}$@ox-CF**, e) **Co$_{ex}^{\text{heptOH}}$@CF** and f) **Co$_{ex}^{\text{heptOH}}$@ox-CF**.

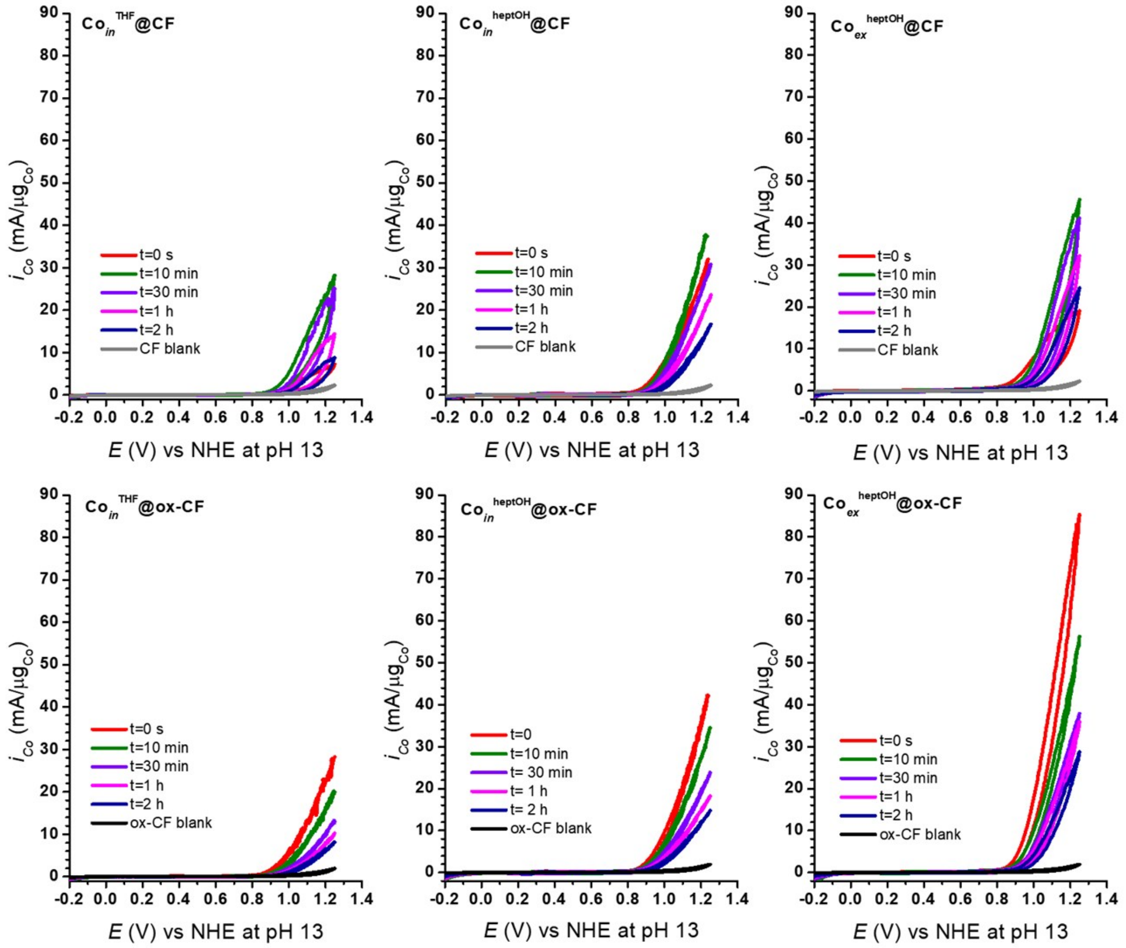

Figure S6. Cyclic Voltammetries (CVs) in a 0.1 M NaOH aqueous solution at pH 13 of 1 mg CFs brush of **Co$_{in}^{\mathrm{THF}}$@CF**, **Co$_{in}^{\mathrm{THF}}$@ox-CF**, **Co$_{in}^{\mathrm{heptOH}}$@CF**, **Co$_{in}^{\mathrm{heptOH}}$@ox-CF**, **Co$_{ex}^{\mathrm{heptOH}}$@CF** and **Co$_{ex}^{\mathrm{heptOH}}$@ox-CF**. CF blanks in grey, ox-CF blanks in black, CV at t=0 s in red, CV after 10-min CA in green, CV after 30-min CA in purple, CV after 1-h CA in pink and CV after 2-h CA in blue.

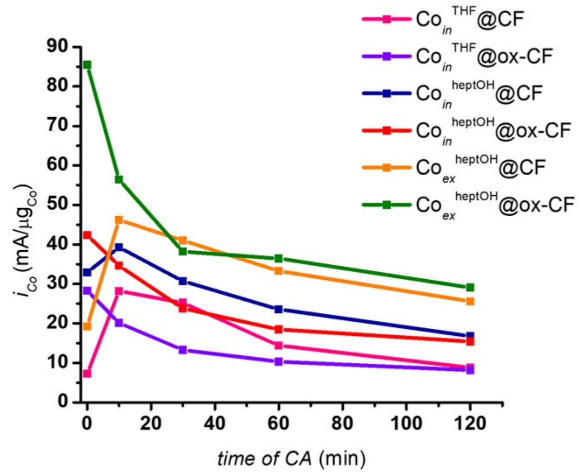

Figure S7. Evolution of the i_{Co} *vs.* time of CA in a 0.1 M NaOH aqueous solution at pH 13 of 1 mg CFs brush of **Co$_{in}^{\mathrm{THF}}$@CF**, **Co$_{in}^{\mathrm{THF}}$@ox-CF**, **Co$_{in}^{\mathrm{heptOH}}$@CF**, **Co$_{in}^{\mathrm{heptOH}}$@ox-CF**, **Co$_{ex}^{\mathrm{heptOH}}$@CF** and **Co$_{ex}^{\mathrm{heptOH}}$@ox-CF**.

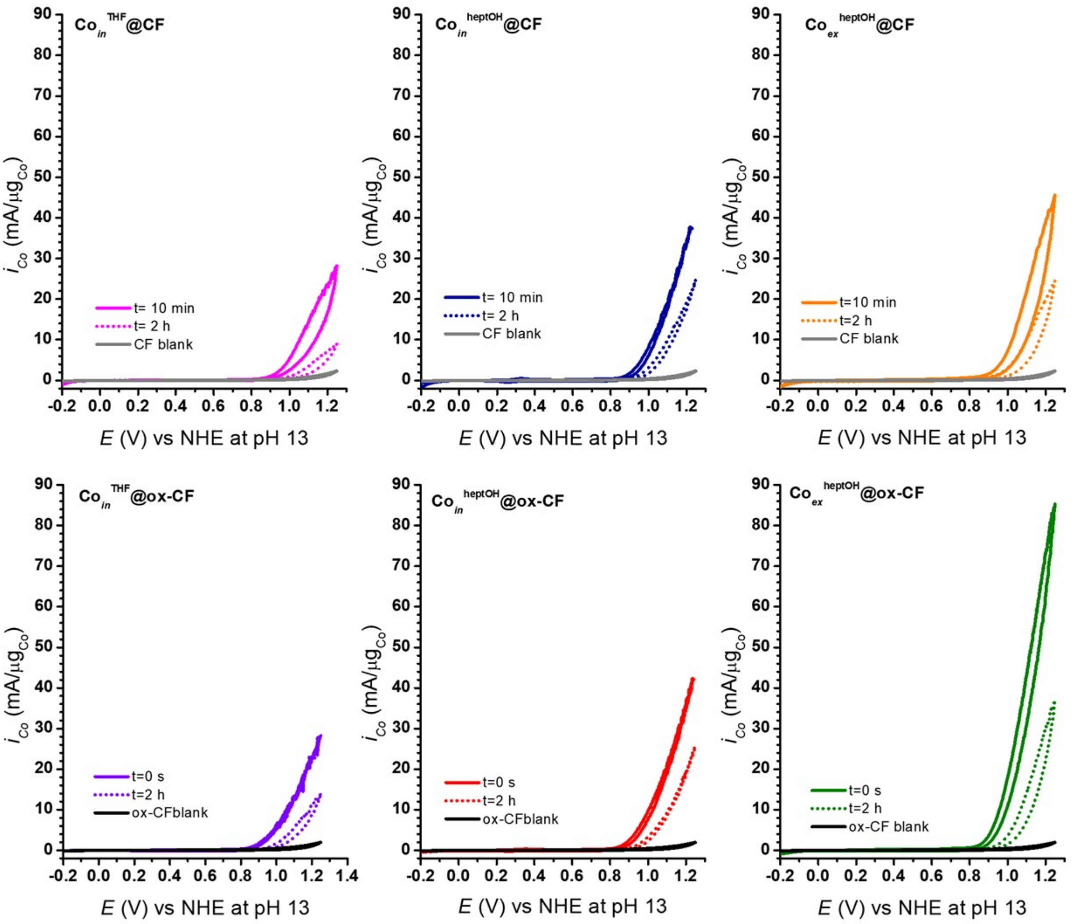

Figure S8. CVs for **Co$_{in}^{THF}$@CF** (pink), **Co$_{in}^{THF}$@ox-CF** (purple), **Co$_{in}^{heptOH}$@CF** (blue), **Co$_{in}^{heptOH}$@ox-CF** (red), **Co$_{ex}^{heptOH}$@CF** (orange) and **Co$_{ex}^{heptOH}$@ox-CF** (green) recorded before and after a 2-h chronoamperometry experiment in a 0.1 M NaOH aqueous solution (pH 13). i_{Co} t=2h measured after removing all the bubbles formed on the system and performing IR drop correction at 85% again. Ox-CF (black) and CF (grey) blanks are also displayed. Chronoamperometries were performed at a fixed potential of 1 V vs NHE at pH 13 (η = 537 mV) for 2 h in order to study the stability of the systems.

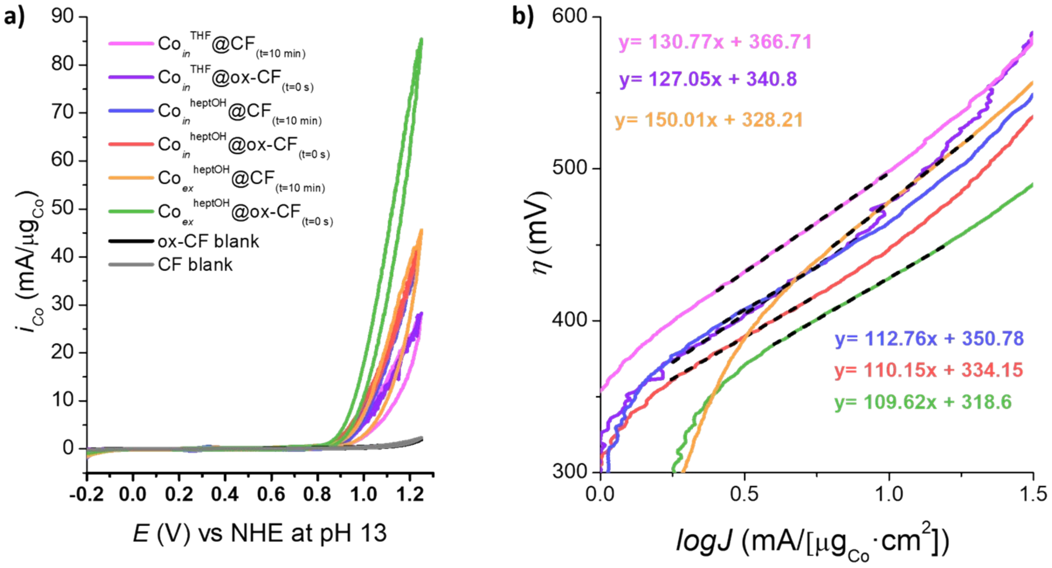

Figure S9. a) Cyclic Voltammograms (CVs) in a 0.1 M NaOH aqueous solution at pH 13 of ox-CFs at t = 0 s and of CFs at t = 10 min (after activation). **Co$_{in}^{THF}$@CF** (pink), **Co$_{in-}^{THF}$@ox-CF** (purple), **Co$_{in}^{heptOH}$@CF** (blue), **Co$_{in}^{heptOH}$@ox-CF** (red), **Co$_{ex}^{heptOH}$@CF** (orange) and **Co$_{ex}^{heptOH}$@ox-CF** (green). ox-CF (black) and CF (grey) blanks are also shown. b) Tafel plots of all ox-CFs at t = 0 s and all CFs at t = 10 min (after activation) (colour code as in a).

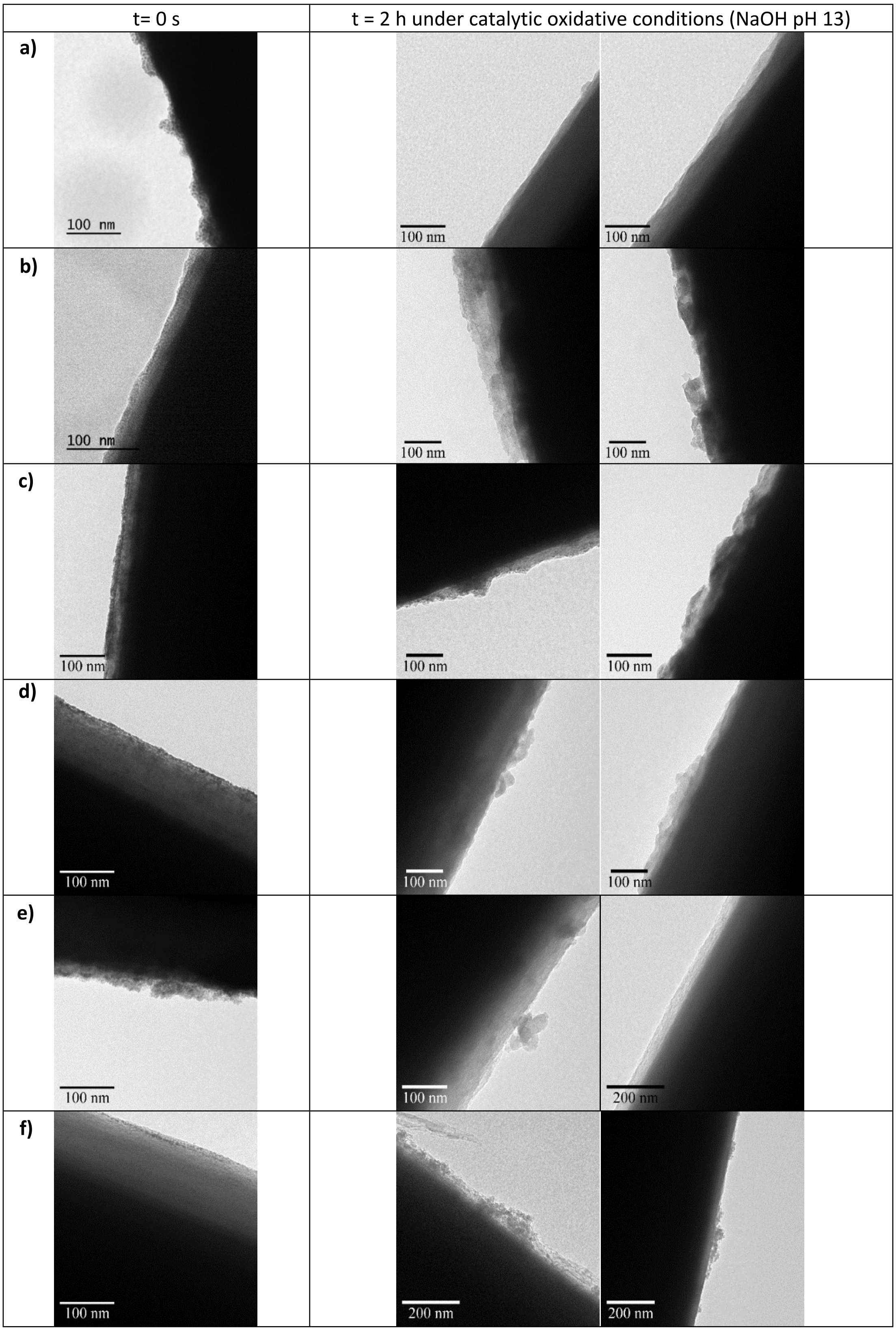

Figure S10. Representative TEM images of a) **Co$_{in}^{\text{THF}}$@CF**, b) **Co$_{in}^{\text{THF}}$@ox-CF**, c) **Co$_{in}^{\text{heptOH}}$@CF**, d) **Co$_{in}^{\text{heptOH}}$@ox-CF**, e) **Co$_{ex}^{\text{heptOH}}$@CF** and f) **Co$_{ex}^{\text{heptOH}}$@ox-CF** at t=0 s and t=2 h after a chronoamperometry at 1 V vs NHE (i.e. η =537 mV) in 0.1 M NaOH (pH 13).

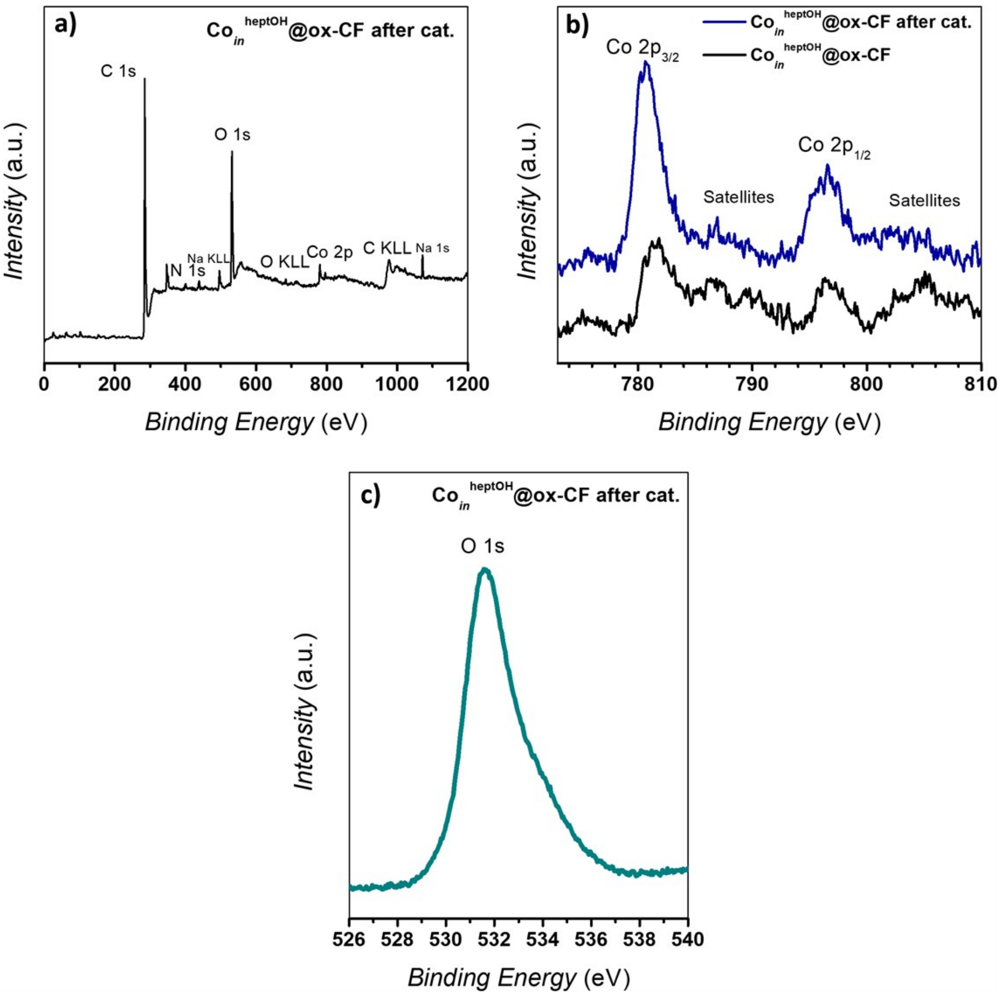

Figure S11. a) XPS survey of **Co$_{in}^{heptOH}$@ox-CF** after a 2 h chronoamperometry (1 V vs. NHE, 0.1 M NaOH). The main peaks can be clearly indexed to O 1s, N 1s and C 1s regions (O KLL represents the energy of the electrons ejected from the atoms due to the filling of the O1s state (K shell) by an electron from the L shell coupled with the ejection of an electron from an L shell). b) Comparison of high-resolution XPS analysis in the Co 2p region for **Co$_{in}^{heptOH}$@ox-CF** before (black line) and after (blue line) a 2 h chronoamperometry. c) O 1s XPS high-resolution spectra for **Co$_{in}^{heptOH}$@ox-CF** after a 2 h chronoamperometry.

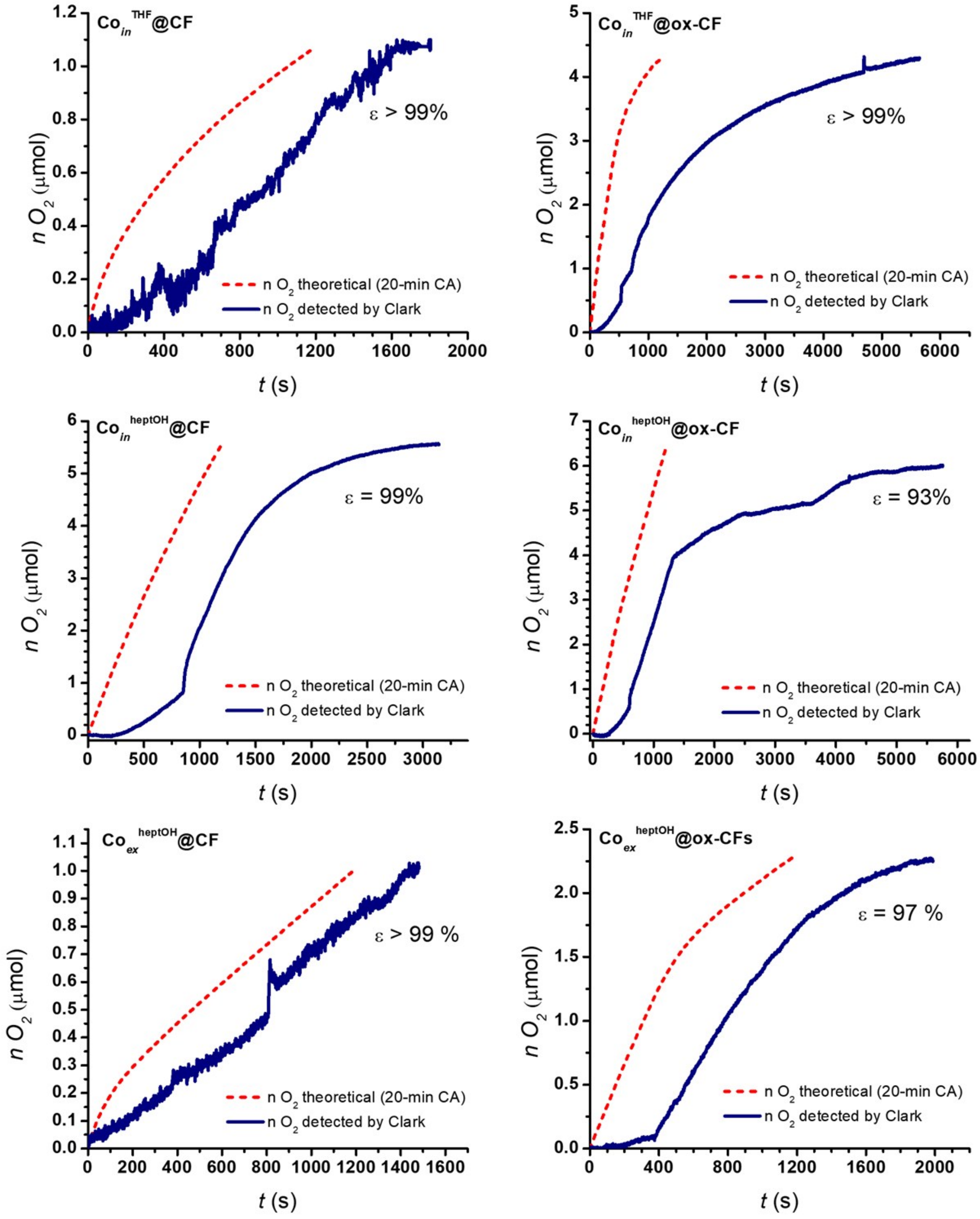

Figure S12. O_2-monitored chronoamperometry experiments for Faradaic efficiency determination. A fixed potential of 1 V vs NHE (pH 13) was applied for 20 min in the CA experiments.

Table S1. Binding energies (eV) of core electrons and satellites of CFs-supported Co-based NPs.

Sample	**Co 2p$_{3/2}$**	**Satellites**	**Co 2p$_{1/2}$**	**Satellites**
Co$_{in}^{THF}$@CF	781.4 eV	785.4 eV	797.3 eV	800.8 eV
Co$_{in}^{THF}$@ox-CF	781.5 eV	785.4 eV	797.3 eV	802.9 eV
Co$_{in}^{heptOH}$@CF	781.7 eV	785.6 eV	797.4 eV	803.0 eV
Co$_{in}^{heptOH}$@ox-CF	781.6 eV	786.9 eV	796.9 eV	804.3 eV
Co$_{in}^{heptOH}$@ox-CFs after catalysis	780.9 eV	786.2eV	796.4 eV	802.6 eV
Co$_{ex}^{heptOH}$@CF	781.2 eV	785.9eV	797.4 eV	804.2 eV
Co$_{ex}^{heptOH}$@ox-CF	781.0 eV	785.5 eV	797.1 eV	803.1 eV

Table S2. Main data of the progressive deactivation of the systems when successive chronoamperometries at a fixed potential of 1 V vs NHE are performed to each system.

System	**$i_{Co\ t=0\ s}$ (mA/μg$_{Co}$)**	**$i_{Co\ t=10\ min}$ (mA/μg$_{Co}$)**	**$i_{Co\ t=30min}$ (mA/μg$_{Co}$)**	**$i_{Co\ t=1h}$ (mA/μg$_{Co}$)**	**$i_{Co\ t=2h}$ (mA/μg$_{Co}$)**	**$i_{Co\ REM}$[(a)] (%)**
Co$_{in}^{THF}$@CF	7.2	28.2	25.2	14.4	8.8	32
Co$_{in}^{THF}$@ox-CF	28.3	20.1	13.30	10.30	8.2	50
Co$_{in}^{heptOH}$@CF	32.9	39.3	30.7	23.6	16.8	64
Co$_{in}^{heptOH}$@ox-CF	42.3	34.6	23.8	18.5	15.4	62
Co$_{ex}^{heptOH}$@CF	19.2	46.15	41.0	33.3	25.6	55
Co$_{ex}^{heptOH}$@ox-CF	85.5	56.4	38.2	36.4	29.1	43

(a) % $i_{Co\ REM}$ calculated by dividing $i_{Co\ t=2\ h}$ by $i_{Co\ t=0\ s}$ as short-term stability data for ox-CF systems and by dividing $i_{Co\ t=2\ h}$ by $i_{Co\ t=10\ min}$ (value after activation) as short-term stability data for CF systems.

Table S3. Summary of electrocatalytic data for relevant carbon-supported Co-based OER electrocatalysts in alkaline media.

Entry	Catalyst	Ø (nm)	η_0 (mV)	Tafel slope (mV/dec)
1[2]	Co_3O_4/BCNO	20 nm	295	57.58
	Co_3O4 + BCNO		390	93.91
	Co_3O_4		380	98.81
2[3]	Co@C	100-400	295^b	58
3[4]	CoP NP/C	25nm	320^b	99
	CoP NR/C		270^b	71
4[5]	Amorphous $Co(OH)_2$ Nanosheet	-	320^c	68
	Crystalline $Co(OH)_2$		330^c	102
	Co_3O_4		400^c	84
5[6]	Co_3O_4-NC/Gr-12h	50-80± 3	220^b	95
	Co_3O_4-NC/NGr-12h	50 ± 3	200^b	69
6[7]	CG-CoO	10-30 nm	320^b	75
	N-CG-CoO	10-30 nm	270^b	71
7[8]	Co_3O_4/N-rmGO	4-8 nm	295^c 270^b	67^b
	Co_3O_4/rmGO	12-25 nm	270^b	68
8[9]	CoP NPs	1.5-2 nm	350^d	80
	CoP-CNT		290^d	50
9[10]	$Co(TCNQ)_2$/CFs		295^b	188
	$Co(OH)_2$-TCNQ/CFs		280^b	101
10[11]	Co_3O_4/N-p-MCNTs 1	<10nm	295^c	98
	Co_3O_4/N-p-MCNTs 2		245^c	78
	Co_3O_4/p-MCNTs		370^c	114
11[12]	Yolk-Shell Co-CoO/BC	74 nm	280^b	73.3
	Solid Co-CoO/BC		380^b	93.1
12[13]	Co@NC-G-500		390^b	125.6
	Co@NC-G-600		340^b	116.4
	Co@NC-G-700		270^b	73.7
	Co@NC-G-800		290^b	82.5
13[14]	Co@GDY/Co	<10 nm	300^c	148
	Co@GDY		400^c	222

Electrolyte: (^{a}) 0.1 M potassium phosphate pH 7, (^{b}) 1 M KOH pH 14, (^{c}) 0.1 M KOH pH 13 and (^{d}) 0.1 M NaOH pH 13

References

---

[1] J. De Tovar, N. Romero, S. A. Denisov, R. Bofill, C. Gimbert-Suriñach, D. Ciuculescu-Pradines, S. Drouet, A. Llobet, P. Lecante, V. Colliere, Z. Freixa, N. McClenaghan, C. Amiens, J. García-Antón, K. Philippot, X. Sala, *Mater. Today Energy* 2018, **9**, 506-515.

[2] X. Ji, Y. Li, X. Jia, X. Yang, L. Li, Y. Yao, Y. Cheng, X. Zhang, Z. Lu, H. Liu, *J. Electrochem. Soc.* **2019**, 166, H177-H181.

[3] Q. Xiao, Y. Zhang, X. Guo, L. Jing, Z. Yang, Y. Xue, Y-M Yan, K. Sun, *Chem. Commun.* **2014**, 50, 13019-13022.

[4] J. Chang, Y. Xiao, M. Xiao, J. Ge, C. Liu, W. Xing, *ACS. Catal.* **2015**, 5, 6874-6878.

[5] Y. Q. Gao, H. B. Li, G. W. Yang, *J. Appl. Phys*. **2016**, 119, 034902.

[6] S. K. Singh, V. M. Dhavale, S. Kurungot, *ACS Appl. Mater. Interfaces* **2015**, 7, 442-451.

[7] S. Mao, Z. Wen, T. Huang, Y. Hou, J. Chen, *Energy Environ. Sci.* **2014**, 7, 609-616.

[8] Y. Liang, Y. Li, H. Wang, J. Zhou, J. Wang, T. Regier, H. Dai, *Nature Materials* **2011**, 10, 780- 786.

[9] C. C. Hou, S. Cao, W.F. Fu, Y. Chen, *ACS Appl. Mater. Interfaces* **2015**, 7, 2412-28419.

[10] D. Wu, Y. Wei, X. Ren, X. Li, Y. Liu, X. Guo, Z. Liu, A. M. Asiri, Q. Wei, X. Sun, *Adv. Mater*. **2018**, 1705366.

[11] Z. Huang, X. Qin, G. Li, W. Yao, J. Liu, N. Wang, K. Ithisuphalp, G. Wu, M. Shao, Z. Shi, *ACS Appl. Energy Mater.* **2019**, 2, 4428-4438.

[12] M. Yang, D. Wu, D. Cheng, *Int. J. Hydrog. Energy* **2019**, 44, 6525-6534.

[13] X. Wen, X. Yang, M. Li, L. Bai, J. Guan, *Electrochim Acta* **2019**, 296, 830-841

[14] J. Li, X. Gao, X. Jiang, X. B. Li, Z. Liu, J. Zhang, C. H. Tung, L. Z. Wu, *ACS Catal.* **2017**, 7, 5209-5213.